Solar Energy Materials & Solar Cells 111 (2013) 16–22

Contents lists available at SciVerse ScienceDirect

Solar Energy Materials & Solar Cells

journal homepage: www.elsevier.com/locate/solmat

Enhanced performance in bulk heterojunction solar cells by introducing naphthalene derivatives as processing additives

Soo Won Heo, Seung Hee Kim, Eui Jin Lee, Doo Kyung Moon *

Department of Materials Chemistry and Engineering, Konkuk University, 1 Hwayang-dong, Gwangjin-gu, Seoul 143-701, Republic of Korea

ARTICLE INFO

Article history:
Received 10 July 2012
Received in revised form
13 December 2012
Accepted 14 December 2012
Available online 19 January 2013

Keywords:
Polymer solar cells (PSCs)
Processing additives
P3HT
PL quenching
Crystallinity

ABSTRACT

Naphthalene derivatives such as 1-fluoronaohthalene, 1-chloronaohthalene, 1-bromonaohthalene, and 1-iodonaohthalene were introduced to poly (3-hexylthiophene) (P3HT): [6,6]-phenyl-C_{61}-butyric acid methyl ester (PCBM)-based bulk heterojunction (BHJ) polymer solar cells (PSCs) as processing additives. To investigate why the addition of naphthalene derivatives improved the efficiency of PSCs, the photon absorbance properties were observed using UV–vis spectroscopy and photoluminescence (PL). Then, the degree of crystallinity of P3HT was examined through X-ray diffraction (XRD) analysis. In addition, changes in the nanostructure and surface morphology of the P3HT:PC_{61}BM blend film were observed through atomic force microscopy (AFM) and transmission electron microscopy (TEM). The series resistance (R_S) and shunt resistance (R_{SH}) of the fabricated PSCs were 8.77 $\Omega\,cm^2$ and 2337 $\Omega\,cm^2$, respectively. The short circuit current density (J_{SC}), open circuit voltage (V_{OC}), and fill factor (*FF*) were 9.7 mA/cm^2, 0.636 V, and 63.6%, respectively. As a result, the power conversion efficiency (PCE) was 3.9%.

1. Introduction

Polymer solar cells (PSCs) based on conjugated polymers have advantages of good mechanical properties and easy fabrication, and enable the fabrication of light-weight devices [1–3]. Techniques such as spin-coating, ink-jet printing, roll-to-roll printing, brush painting, or stamping can be applied to flexible substrates to produce light-weight, flexible, large-area photovoltaic devices at low cost [4–9]. More than a decade of development has raised the maximum power conversion efficiency (PCE) of PSCs to about 6–7% [10,11]. Therefore, many studies have been conducted on the design of new, low-band-gap polymer materials in order to improve PCE [12,13], the development of novel device fabrication methods and structures [14,15], and the introduction of bulk heterojunction (BHJ) systems and understand BHJ device physics [16].

BHJ PSCs are applied to the photoactive layer after blending an electron-donating material (p-type conjugated polymers) with an electron-accepting material (n-type fullerene derivatives). To improve the PCE of BHJ PSCs, continuous pathways must be formed to allow excited electrons and holes to be transferred to an external circuit without being recombined with each other. Typical BHJ PSCs comprise a system of poly (3-hexylthiophene) (P3HT) as an electron donor, and [6,6]-phenyl-C_{61}-butyric acid methyl ester (PCBM) as an electron acceptor. In this system, PCBM is dispersed among P3HT chains, and prevents P3HT from being crystallized. Therefore, untreated BHJ PSCs have low PCE (ca. 1–2%). Therefore, in order to improve the PCE of P3HT/PCBM BHJ PSCs, P3HT and PCBM should exist in an interpenetrating network form, and should be very well phase-separated. The efficiency has been improved in several studies by thermally annealing the BHJ films to form a well-defined bicontinuous interpenetrating network between P3HT and PCBM [17]. Padinger et al. achieved a PCE of 3.5% by using thermal annealing to improve the morphology of the BHJ film [18]. Ma et al. also improved the PCE up to ca. 5.1% through post-thermal annealing [19].

As in other methods, device performance was enhanced by controlling the physical behavior of the polymer blend through a solvent treatment method. Li et al. improved the PCE by controlling the solvent evaporation rate and film growth rate. This solvent annealing method improved the ordered structure formation of P3HT in the film by providing more time to help the P3HT chains to continue their self-organization process before the P3HT/PCBM solution was turned into a solid film [20]. However, the PCE of this method was restricted to 4.4%.

In addition, Zhang et al. introduced a solvent mixture, which blended two solvents with different boiling [21]. Even though the P3HT chain were reorganized by introducing a solvent mixture to which a small amount of chlorobenzene (CB; b.p. 132 °C) had been added to the host solvent chloroform (b.p. 61 °C), a low PCE of 2.3% was observed. Studies have also been reported on BHJ PSCs with

* Corresponding author. Tel.: +82 2 450 3498; fax: +82 2 444 0765.
E-mail address: dkmoon@konkuk.ac.kr (D.K. Moon).

0927-0248/$ - see front matter © 2012 Elsevier B.V. All rights reserved.
http://dx.doi.org/10.1016/j.solmat.2012.12.027

performance enhanced by adding a few volume percent of processing additives (e.g., 1,8-diiodooctane, and 1,8-octanedithiol) to the host solvent in a similar method [17,22]. These processing additives can improve the degree of crystallinity of the polymer by nanoscale phase-separation of the polymer and PCBM. However, most known processing additives have been applied to cases in which a low-band-gap polymer has been used as an electron donor material. In the P3HT/PCBM system, alkanethiols such as 1,8-octanedithiol have been used to decrease the degree of crystallinity of P3HT, because they have an impact on the nanoscale phase separation of P3HT/PCBM by aggregating P3HT.

This study introduces naphthalene derivatives as novel processing additives to the P3HT/PCBM system, in order to dramatically increase the PCE of PSCs by improving the degree of crystallinity and photon absorption property of the BHJ film. The naphthalene derivatives have a higher b.p. (215–305 °C) than the host solvent CB (132 °C), and are miscible with CB. In addition, because PCBM is more soluble than P3HT in both CB and naphthalene derivatives [23], it can be used to improve the ordering of the polymer domain by adding naphthalene derivatives to CB. The mechanism of this improvement in the properties of BHJ PSCs is determined by observing the optical, electrical, and structural properties of the BHJ film after adding the processing additives. Using UV/photoluminescence (PL) spectroscopy, the absorption of photons and the quenching properties of the excited electrons were observed. The structural properties of P3HT crystallite were analyzed through X-ray diffraction (XRD) pattern analysis. The phase segregation of the P3HT/PCBM film and the increase of crystallinity in P3HT were observed through atomic force microscopy (AFM) and transmission electron microscopy (TEM) analysis.

2. Materials and measurements

2.1. Materials

The indium tin oxide (ITO) glass that was used as the transparent electrode was obtained from Samsung Corning (ITO:170 nm, 10 Ω/sq). Poly(3,4-ethylenedioxythiophene)/poly(styrenesulfonate) (PEDOT:PSS, AI 4083) was purchased from Clevios, and the P3HT used as a donor material in the photoactive layer was purchased from Rieke metal. PCBM, the acceptor material, was purchased from Nano C. CB, which was used as a host solvent, and 1-fluoronaphthalenethiol (1-FN), 1-chloronaphthalene (1-CN), 1-bromonaphthalene (1-BN) and 1-iodonaphthalene (1-IN), which were used as processing additives, were purchased from Aldrich. The chemical structure of P3HT, PCBM, and the processing additives are shown in Fig. 1.

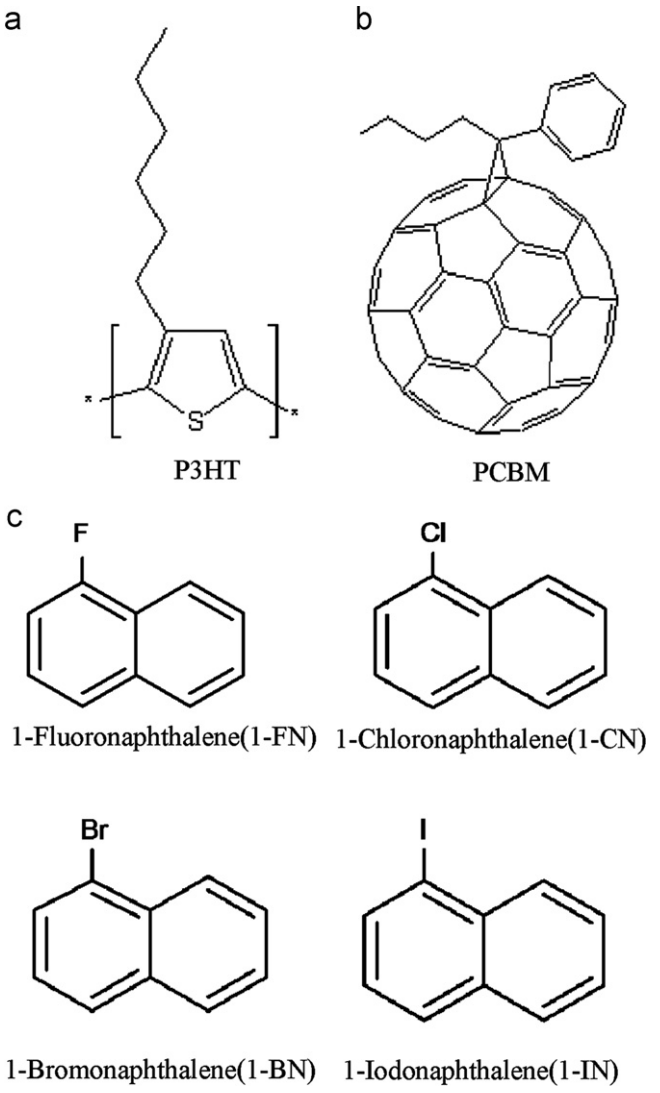

Fig. 1. Chemical structure of (a) P3HT, (b) PCBM and (c) processing additives.

2.2. Measurements

All of the thin films were fabricated using a GMC2 spin coater (Gensys), and their thicknesses were measured using an alpha step 500 surface profiler (KLA-Tencor). The photon absorption property and quenching property of the excited electrons in the BHJ film were measured with UV–vis spectroscopy (HP Agilent 8453) and PL spectroscopy (Perkin Elmer LS 55 luminescence spectrometer), respectively. The XRD patterns were observed using a Rigaku D/MAX 2200 diffractometer with CuK_α radiation to confirm the crystalline size of P3HT. The morphology of the BHJ films was observed through AFM (PSIA XE-100) and FE-TEM (FEI Tecnai G2 F30), respectively. The surface energy was measured with a contact-angle meter (KRUSS K6). The current density–voltage (J–V) characteristics of the PSCs were measured using a Keithley 2400 source measure unit. The devices were evaluated at 298 K using a Class A Oriel solar simulator (Oriel 96000 150W solar simulator) with an xenon lamp to simulate AM 1.5G irradiation (100 mw/cm^2) with a wavelength from 400 to 1100 nm. The instrument was calibrated with a monocrystalline Si diode fitted with a KG5 filter to bring the spectral mismatch to unity. The calibration standard was calibrated by the National Renewable Energy Laboratory (NREL). IPCE (Mc science) was measured against the best-performance device.

3. Experimental

3.1. Cleaning of patterned ITO glass

To clean the patterned ITO glass, it was sonicated for 20 min. in detergent (Alconox® in deionized water, 10%), acetone, isopropyl alcohol, and deionized water, in that order. The moisture was removed by N_2 gas flow. To ensure complete removal of all of the remaining water, the patterned ITO glass was baked on a hot plate for 10 min at 100 °C. For hydrophilic treatment of the patterned ITO glass, it was cleaned for 10 min in a UVO cleaner.

3.2. Fabrication of PSCs

PEDOT:PSS was spin coated from aqueous solution to form a 40-nm-thick film on the patterned ITO glass. The substrate was dried for 20 min at 120 °C in air and then transferred into a glovebox

to spin coat the active layer. A solution containing a mixture of P3HT/PCBM (1:0.6) in CB with or without various concentrations of processing additives (1-FN, 1-BN, 1-CN and 1-IN) was then spin coated on top of the PEDOT:PSS layer to produce a 130-nm-thick photoactive layer that was then vacuum treated at 1×10^{-6} Torr for 60 min. To form the cathode, BaF_2 (0.1 Å/s, 2 nm), Ba (0.2 Å/s, 2 nm), and Al (5 Å/s, 100 nm) were thermally deposited in order, in a high-vacuum chamber. Finally, PSCs with an active area of 4 mm^2 (2 mm × 2 mm) were fabricated through encapsulation.

4. Results and discussion

Fig. 2 shows the *J–V* curve and external quantum efficiency (EQE) when naphthalene derivatives were added as processing additives, and the results are presented in Table 1. The optimized concentration of the processing additive was 2 vol%. When 1-BN was added as the processing additive, the open circuit voltage (V_{OC}), short circuit current density (J_{SC}), and fill factor (*FF*) were 0.636 V, 9.7 mA/cm^2, and 63.6%, respectively. The calculated PCE of 3.9% was increased by 56% compared to the reference. The EQE maximum value was 56% at −560 nm. In addition, the PCE of the devices to which 1-CN and 1-FN were added were 3.7% and 3.4%, which were increased by 48% and 36%, respectively. However, the PCE of the device to which 1-IN had been added was 2.3%, which was slightly less efficient than the reference. In the devices with

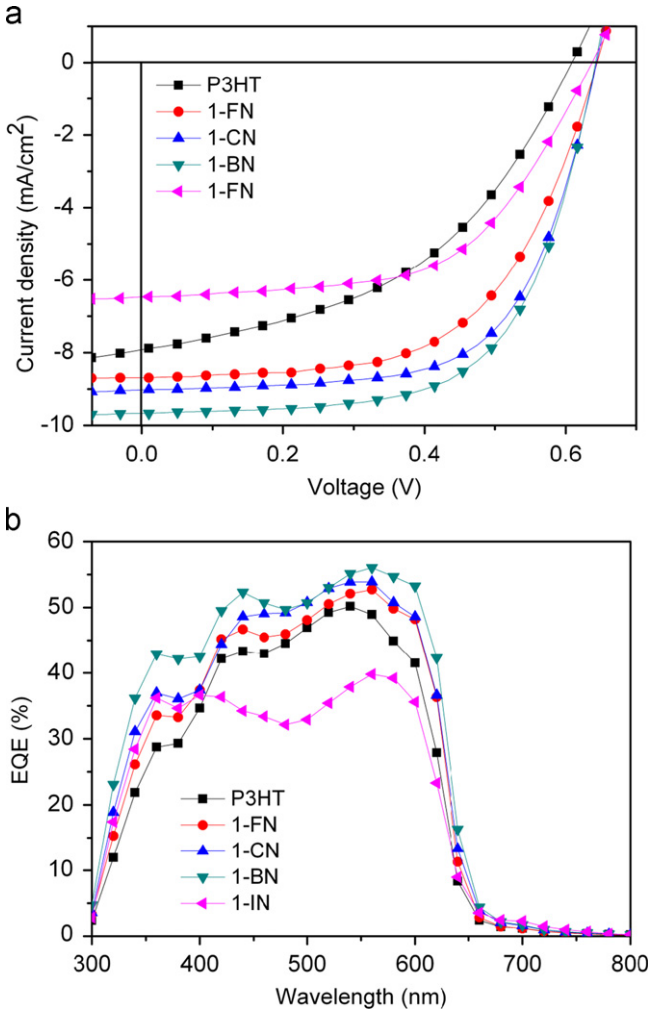

Fig. 2. (a) *J–V* characteristics and (b) external quantum efficiency (EQE) characteristics of P3HT:PCBM=1:0.6 composite films with various processing additives.

Table 1
Photovoltaic performances of BHJ PSCs composed of P3HT:PCBM fabricated with various processing additives.

Additive	J_{SC} [mA/cm^2]	V_{OC} [*V*]	*FF* [%]	PCE [%]	R_S [Ω cm^2]	R_{SH} [Ω cm^2]
P3HT(Ref)	7.5	0.636	52.7	2.5	19.61	704
1-FN	8.7	0.636	61.0	3.4	8.97	1234
1-CN	9.0	0.636	64.5	3.7	8.69	1807
1-BN	9.7	0.636	63.6	3.9	8.77	2337
1-IN	6.5	0.636	57.0	2.3	23.25	1263

ITO(170 nm)/PEDOT:PSS(40 nm)/P3HT:PCBM:additive(130 nm)/BaF_2(2 nm)/Ba(2 nm)/Al(100 nm)

an improved efficiency due to the addition of a processing additive, both J_{SC} and *FF* improved compared to the reference, but V_{OC} remained unchanged. To investigate the causes of these results, the series resistance (R_S) and shunt resistance (R_{SH}) were measured in each device (Table 1). When 1-BN was added, R_S was 8.77 Ω cm^2, which was decreased by about 2.2-fold compared to the reference (19.61 Ω cm^2). In addition, R_{SH} was 2337 Ω cm^2, which was increased by about 3.3-fold compared to the reference (704 Ω $cm^{2)}$). Therefore, the addition of 1-BN increased both J_{SC} and *FF* [9]. These patterns were also observed in the devices to which 1-FN and 1-CN were added, because the three different processing additives added to the photoactive layer changed its photon absorption, nanostructure, and surface morphology.

Fig. 3 shows the photon absorption properties with the addition of processing additives, which were observed using UV–vis spectroscopy. Fig. 3(a) shows the UV–vis spectrum of the device to which 1-FN, 1-CN, 1-BN, and 1-IN (2 vol%) were added to the P3HT film as processing additives. When 1-FN, 1-CN, and 1-BN were added, the device was better than P3HT in terms of photon absorption properties. Fig. 3(b) shows the UV–vis spectrum of the device to which 1-FN, 1-CN, 1-BN, and 1-IN (2 vol%) were added to the P3HT-PCBM blended film as processing additives. When 1-BN was added, λ_{max} was red-shifted from 495 to 502 nm with an increase in absorbance from 545 to 600 nm, because of the π–π^* transition among the P3HT molecules [24]. This suggests that the crystallinity was improved compared to that of the P3HT:PCBM film, to which processing additive was not added, and hence, the XRD pattern was analyzed for confirmation.

To investigate the ordering of the P3HT chain induced by the addition of the processing additives, the XRD pattern is shown in Fig. 4. The intensity of the (1 0 0) diffraction peak was increased at $2\theta = 4.8^\circ$ in the film to which 1-FN, 1-CN, and 1-BN were added, compared to the P3HT:PCBM blended film. An ordered lamellar structure with an interlayer spacing originating from the interdigitated alkyl chains of P3HT was observed in the annealed films [25]. Moreover, the increased intensity indicated an increased crystallinity in P3HT, and hence that the processing additives affected the phase separation of P3HT and PCBM. As a result, the crystallinity of P3HT increased. The crystalline size of P3HT was calculated by using Scherrer's equation, $L = K\lambda/B\cos\theta$, where *L* is the average crystalline size of P3HT (1 0 0), *B* is the full width at half maximum (FWHM) of the (1 0 0) peak, λ is the wavelength of the incident X-rays (0.154 nm), θ is the angle of refraction, and *K* is Scherrer's constant (0.9). Based on Scherrer's equation, the crystalline size of each P3HT is stated in Table 2. In P3HT to which no processing additive had been added, the crystalline size was about 19 nm. However, it gradually increased when 1-FN and 1-CN were added. The addition of 1-BN increased the size up to 26 nm. This increase of P3HT crystalline size was attributed to the improved carrier mobility that was created in the photoactive layer. Consequently, the J_{SC} and *FF* of PSCs were improved, and PCE was also thus improved. However, when 1-IN was added, the crystalline size decreased to 17 nm, which indicated a decreased carrier mobility. Compared to the other processing additives, 1-IN

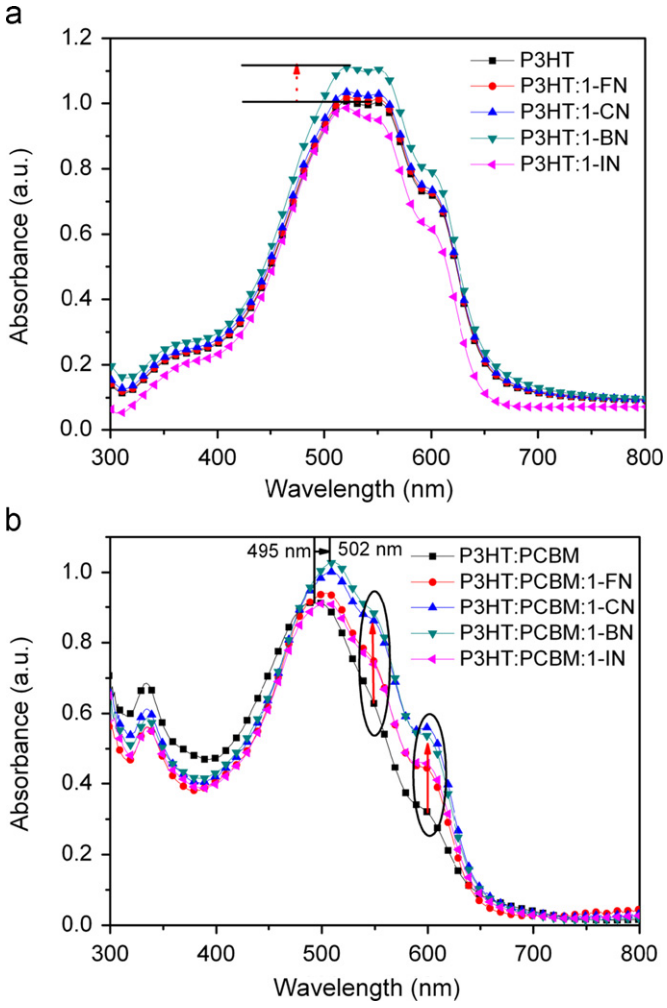

Fig. 3. UV–vis absorption spectra of (a) P3HT films with/without processing additives, and (b) P3HT:PCBM blending films with/without processing additives.

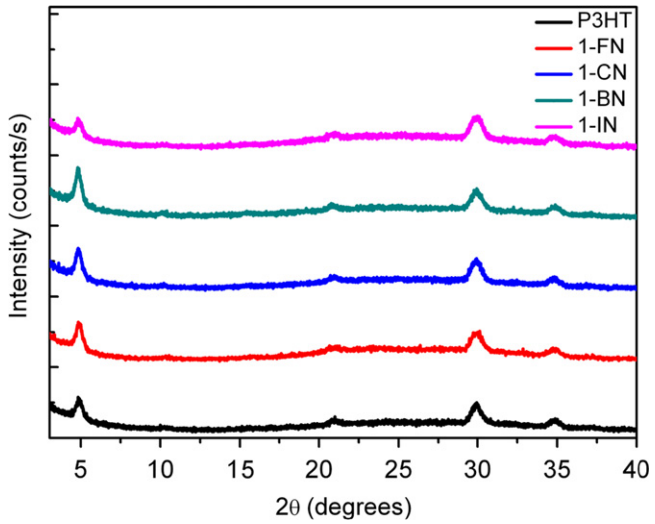

Fig. 4. X-ray diffraction (XRD) patterns of P3HT:PCBM blend films with/without processing additives.

has a high b.p. (305 °C), but a vapor pressure (v.p.) that is 10 to 100-fold lower at 0.0018 mmHg (Table 3). This suggests that 1-IN was not completely removed during the vacuum treatment and that its remnant interrupted the crystallization of P3HT.

Table 2
Crystalline size of P3HT.

Processing additives	Crystalline size of P3HT (nm)
None	19
1-FN	22
1-CN	23
1-BN	26
1-IN	17

Table 3
Boiling points and vapor pressures of chlorobenzene solvent and various processing additives.

Solvent and processing additives	Boiling point (b.p./°C)	Vapor pressure (v.p./mmHg)
Chlorobenzene	132	8.8 (at 20 °C)
1-FN	215	0.221 (at 25 °C)
1-CN	263	0.02 (at 25 °C)
1-BN	280	0.017 (at 20 °C)
1-IN	302	0.0018 (at 25 °C)

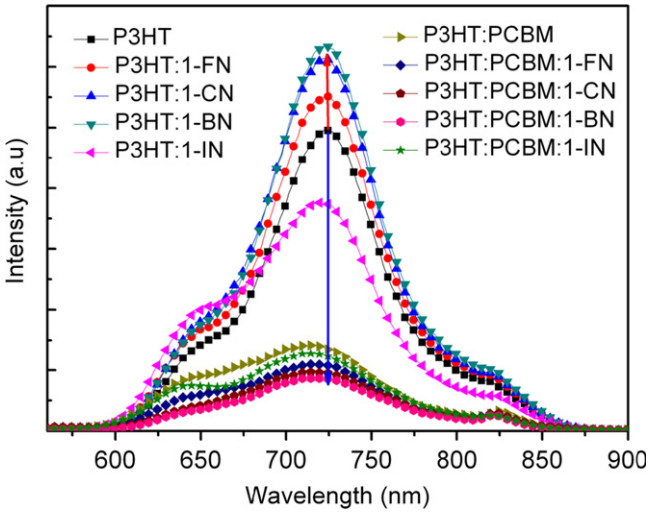

Fig. 5. PL quenching data of P3HT films with/without processing additives and P3HT:PCBM blend films with/without processing additives.

Table 4
Calculated PL quenching area.

Processing additive	Quenching area (%)
None	67
1-FN	75
1-CN	80
1-BN	84
1-IN	57

Consequently, the J_{SC} of the fabricated PSCs decreased, which in turn decreased PCE as well.

Fig. 5 shows the PL quenching in order to determine whether the excitons that were generated on the photoactive layer were efficiently dissociated As the quenched amount increases, the efficiency of electron-hole dissociation improves. As shown in

Table 4, 67% of the quenching ratio was observed in the P3HT to which no processing additives had been added in the photoactive layer. In comparison, quenched ratios of 84%, 75%, and 80% were detected when 1-BN, 1-FN, and 1-CN were added, respectively, indicating a maximum increase of 17% for 1-BN. These quenched ratios were all greater than that of P3HT. When 1-IN was added, however, the quenched area decreased by 10% to 57%. The addition of processing additives improved the absorption properties by causing π–π^* transition among the P3HT molecules, and promoted carrier mobility by increasing the crystallinity in P3HT. The ability to absorb more photons without the processing additives allowed them to be transferred quickly to the external circuit without having to prevent them from being recombined. To investigate the effect of the processing additives on the structural properties of the BHJ-structured photoactive layer, AFM and TEM analyses were performed. Fig. 6 shows the changes observed through AFM in the surface morphology induced by the presence or absence and type of processing additive in the

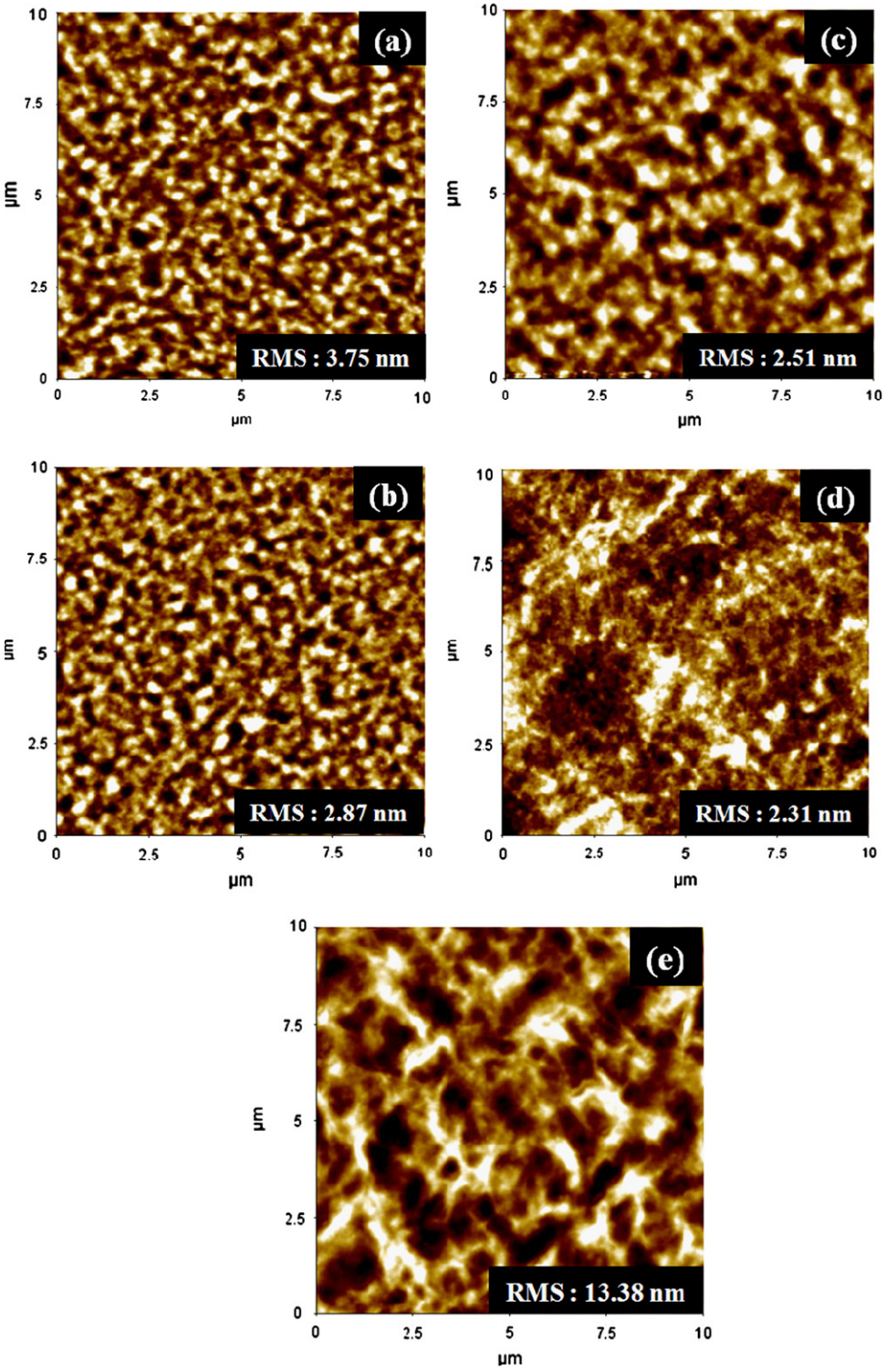

Fig. 6. AFM images of films cast from P3HT:PCBM with/without processing additives: (a) P3HT:$PC_{61}BM$, (b) 1-FN, (c) 1-CN, (d) 1-BN and (e) 1-IN.

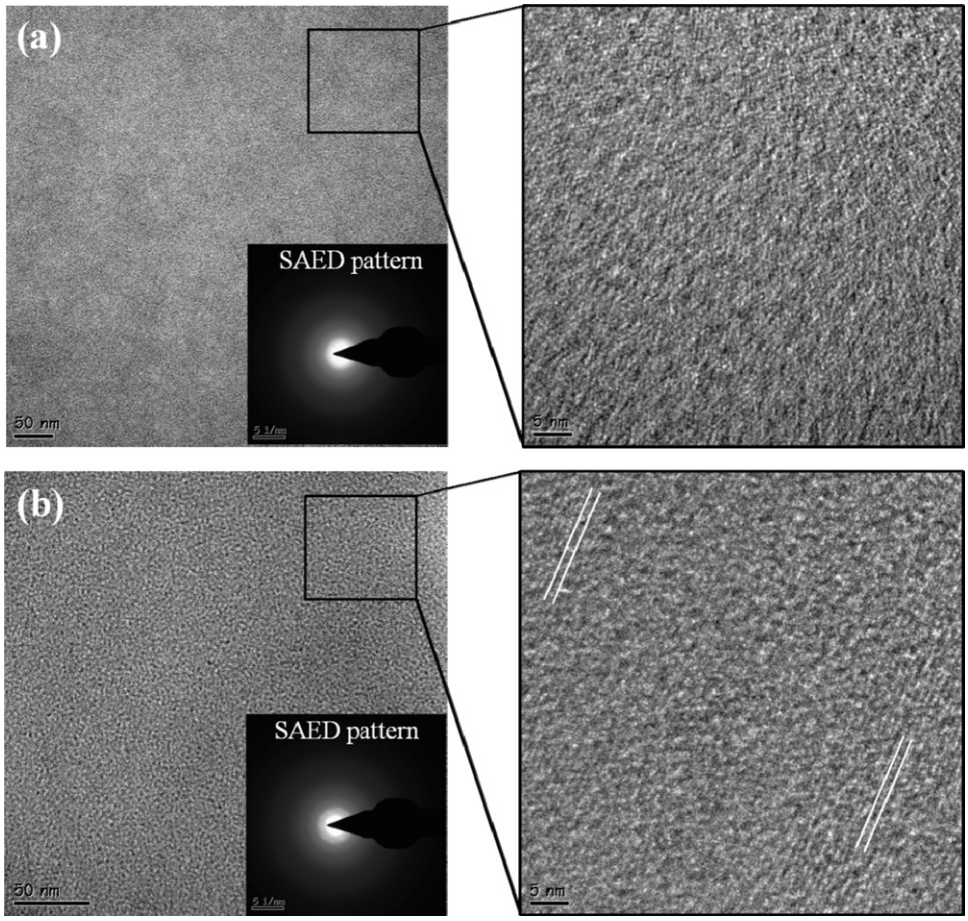

Fig. 7. TEM of films cast from P3HT:PCBM (a) without processing additive (inset: SAED pattern) and (b) with 1-BN (inset: SAED pattern).

P3HT:PCBM films. The root mean square (RMS) roughness of the device to which 1-BN had been added (2.31 nm) was lower than that of the device without any processing additive (3.75 nm). This confirmed that the addition of 1-BN improved the donor-acceptor phase separation, leading to the formation of a nanoscale domain. The addition of 1-CN also improved the phase separation and induced the formation of a nanoscale domain, because the processing additives such as 1-BN have a selective solubility with PCBM. In addition, because it has higher b.p. and lower v.p. compared to CB, the CB-dissolved donor P3HT initially formed a film during vacuum treatment, after which the acceptor-dissolved processing additive formed a nanoscale domain, which facilitated effective phase separation. The addition of processing additives allowed the nanoscale domain to provide a pathway through which holes and electrons that had been separated after forming an interpenetrating network could be transferred to the cathode, increase J_{SC}, and prevent them from being recombined while the carriers are moving. Therefore, R_S decreased while R_{SH} increased in the devices to which any processing additives other than 1-NT had been added. As a result, both J_{SC} and *FF* were improved. The addition of 1-IN, however, led to the formation of a large domain. The RMS of 13.38 nm confirmed that the domains were aggregated. Due to the failure to form a bicontinuous network, J_{SC} was decreased, and the efficiency was not improved.

Fig. 7 shows TEM images of a thin film in which 2 vol% of 1-BN had been added to P3HT:PCBM and P3HT:PCBM. Because PCBM has a greater electron scattering density than P3HT in the TEM images, it is expressed in dark areas [26]. The P3HT:PCBM thin film (b) to which 1-BN had been added was wider than the P3HT:PCBM thin film (a) in terms of dark area distribution. This result confirmed the large-scale phase separation. From the selected area electron diffraction (SAED) pattern shown in the inset of Fig. 4(b), the addition of 1-BN also improved the crystallinity in P3HT. Therefore, it was concluded that a nanoscale domain can be formed through the addition of processing additives, and that the separated holes and electrons can be effectively dissociated through large-scale phase separation. Furthermore, the carriers were shown to be quickly transferred because of the polymer crystallinity.

5. Conclusion

In summary, we have dramatically improved the efficiency of fabricated P3HT:PCBM-based PSCs by adding naphthalene derivatives as processing additives. The addition of these processing additives improved the degree of crystallinity of P3HT. In addition, the formation of a nanoscale domain and interpenetrating network has made it possible for a carrier to move quickly to an external circuit, and the absorbance was improved by the resulting increase in photon harvesting properties. As a result, R_S decreased while R_{SH} increased. The PCE was improved by 56% due to the increase in J_{SC} and *FF*.

Acknowledgement

This research was supported by a grant(10037195) from the Fundamental R&D Program for Core Technology of Materials funded by the Ministry of Knowledge Economy, Republic of Korea

and the National Research Foundation of Korea Grant funded by the Korean Government(MEST)" (NRF-2009-C1AAA001-2009-0093526)

References

[1] H.-Y. Chen, J.H. Hou, S.Q. Zhang, Y.Y. Liang, G.W. Yang, Y. Yang, L.P. Yu, Y. Wu, G. Li, Polymer solar cells with enhanced open-circuit voltage and efficiency, Nature Photonics 3 (2009) 649–653.
[2] Y. Liang, Z. Xu, J. Xia, S.-T. Tsai, Y. Wu, G. Li, C. Ray, L. Yu, For the bright future bulk heterojunction polymer solar cells with power conversion efficiency of 7.4%, Advanced Materials 22 (2010) E135–E138.
[3] J.Y. Lee, Y.J. Kwon, J.W. Woo, D.K. Moon, Synthesis and characterization of fluorine–thiophene-based π-conjugated polymers using coupling reaction, Journal of Industrial and Engineering Chemistry 14 (2008) 810–817.
[4] F.C. Krebs, Fabrication and processing of polymer solar cells: a review of printing and coating techniques, Solar Energy Materials and Solar Cells 93 (2009) 394–412.
[5] E. Bundgaard, O. Hagemann, M. Manceau, M. Jørgensen, F.C. Krebs, Low band gap polymers for roll-to-roll coated polymer solar cells, Macromolecules 43 (2010) 8115–8120.
[6] M. Manceau, D. Angmo, M. Jørgensen, F.C. Krebs, ITO-free flexible polymer solar cells: from small model devices to roll-to-roll processed large modules, Organic Electronics 12 (2011) 566–574.
[7] F.C. Krebs, J. Fyenbo, M. Jørgensen, Product integration of compact roll-to-roll processed polymer solar cell modules: methods and manufacture using flexographic printing, slot-die coating and rotary screen printing, Journal of Materials Chemistry 20 (2010) 8994–9001.
[8] S.W. Heo, J.Y. Lee, H.J. Song, J.R. Ku, D.K. Moon, Patternable brush painting process for fabrication of flexible polymer solar cells, Solar Energy Materials and Solar Cells 95 (2011) 3041–3046.
[9] S.W. Heo, K.W. Song, M.H. Choi, T.H. Sung, D.K. Moon, Patternable solution process for fabrication of flexible polymer solar cells using PDMS, Solar Energy Materials and Solar Cells 95 (2011) 3564–3572.
[10] H.Y. Chen, J. Hou, S. Zhang, Y. Liang, G. Yang, Y. Yang, L. Yu, Y. Wu, G. Li, Polymer solar cells with enhanced open-circuit voltage and efficiency, Nature Photonics 3 (2009) 649–653.
[11] T.Y. Chu, J. Lu, S. Beaupré, Y. Zhang, J.R. Pouliot, S. Wakim, J. Zhou, M. Leclerc, Z. Li, J. Ding, Y. Tao, Thieno[3,4-c]pyrrole-4,6-dione and dithieno[3,2-b:2′,3′-d]silole copolymer with a power conversion efficiency of 7.3%, Journal of the American Chemical Society 133 (2011) 4250–4253.
[12] J.Y. Lee, W.S. Shin, J.R. Haw, D.K. Moon, Low band-gap polymers based on quinoxaline derivatives and fused thiophene as donor materials for high efficiency bulk-heterojunction photovoltaic cells, Journal of Materials Chemistry 19 (2009) 4938–4945.
[13] J.Y. Lee, S.W. Heo, H. Choi, Y.J. Kwon, J.R. Haw, D.K. Moon, Synthesis and characterization of 2,1,3-benzothiadiazole-thieno[3,2-b]thiophene-based charge transferred-type polymers for photovoltaic application, Solar Energy Materials and Solar Cells 93 (2009) 1932–1938.
[14] Y. Wang, L. Yang, C. Yao, W. Qin, S. Yin, F. Zhang, Enhanced performance and stability in polymer photovoltaic cells using lithium benzoate as cathode interfacial layer, Solar Energy Materials and Solar Cells 95 (2011) 1243–1247.
[15] J.M. Yun, J.S. Yeo, J. Kim, H.G. Jeong, D.Y. Kim, Y.J. Noh, S.S. Kim, B.C. Ku, S.I. Na, Solution-processable reduced graphene oxide as a novel alternative to PEDOT:PSS hole transport layers for highly efficient and stable polymer solar cells, Advanced Materials 23 (2011) 4923–4928.
[16] P.W.M. Blom, V.D. Mihailetchi, L.J.A. Koster, D.E. Markov, Device physics of polymer: fullerene bulk heterojunction solar cells, Advanced Materials 19 (2007) 1551–1566.
[17] J.K. Lee, W.L. Ma, C.J. Brabec, J. Yuen, J.S. Moon, J.Y. Kim, K. Lee, G.C. Bazan, A.J. Heeger, Processing additives for improved efficiency from bulk heterojunction solar cells, Journal of the American Chemical Society 130 (2008) 3619–3623.
[18] F. Padinger, R.S. Rittberger, N.S. Sariciftci, Effects of postproduction treatment on plastic solar cells, Advanced Functional Materials 13 (2003) 85–88.
[19] W.L. Ma, C.Y. Yang, X. Gong, K. Lee, A.J. Heeger, Thermally stable, efficient polymer solar cells with nanoscale control of the interpenetrating network morphology, Advanced Functional Materials 15 (2005) 1617–1622.
[20] G. Li, V. Shrotriya, J.S. Huang, Y. Yao, T. Moriarty, K. Emery, Y. Yang, High-efficiency solution processable polymer photovoltaic cells by self-organization of polymer blends, Nature Materials 4 (2005) 864–868.
[21] F. Zhang, K.G. Jespersen, C. Bjorstrom, M. Svensson, M.R. Andersson, V. Sundstrom, K. Magnusson, E. Moons, A. Yartsev, O. Inganas, Influence of solvent mixing on the morphology and performance of solar cells based on polyfluorene copolymer/fullerene blends, Advanced Functional Materials 16 (2006) 667–674.
[22] J. Peet, N.S. Cho, S.K. Lee, G.C. Bazan, Transition from solution to the solid state in polymer solar cells cast from mixed solvents, Macromolecules 41 (2008) 8655–8659.
[23] L. Li, H. Tang, H. Wu, G. Lu, X. Yang, Effects of fullerene solubility on the crystallization of poly(3-hexylthiophene) and performance of photovoltaic devices, Organic Electronics 10 (2009) 1334–1344.
[24] S. Jeong, S.H. Woo, H.K. Lyu, Y.S. Han, Effects of a perfluorinated compound as an additive on the power conversion efficiencies of polymer solar cells, Solar Energy Materials and Solar Cells 95 (2011) 1908–1914.
[25] W. Ma, C. Yang, X. Gong, K. Lee, A.J. Heeger, Thermally stable, efficient polymer solar cells with nanoscale control of the interpenetrating network morphology, Advanced Functional Materials 15 (2005) 1617–1622.
[26] X.N. Yang, J. Loos, S.C. Veenstra, W.J.H. Verhees, M.M. Wienk, J.M. Kroon, M.A.J. Michels, R.A.J. Janssen, Nanoscale morphology of high-performance polymer solar cells, Nano Letters 5 (2005) 579–583.